Atmos. Chem. Phys., 18, 311–326, 2018
https://doi.org/10.5194/acp-18-311-2018

Atmospheric Chemistry and Physics
Open Access
EGU

Vertically resolved concentration and liquid water content of atmospheric nanoparticles at the US DOE Southern Great Plains site

Haihan Chen[1], Anna L. Hodshire[2], John Ortega[3], James Greenberg[3], Peter H. McMurry[4], Annmarie G. Carlton[1], Jeffrey R. Pierce[2], Dave R. Hanson[5], and James N. Smith[1]

[1]Department of Chemistry, University of California, Irvine, 92697, USA
[2]Department of Atmospheric Science, Colorado State University, Fort Collins, 80523, USA
[3]National Center for Atmospheric Research, Atmospheric Chemistry Observations & Modeling Laboratory, Boulder, 80307, USA
[4]Department of Mechanical Engineering, University of Minnesota-Twin Cities, Minneapolis, 55455, USA
[5]Department of Chemistry, Augsburg University, Minneapolis, 55454, USA

Correspondence: James N. Smith (jimsmith@uci.edu)

Received: 26 June 2017 – Discussion started: 11 July 2017
Revised: 16 November 2017 – Accepted: 20 November 2017 – Published: 11 January 2018

Abstract. Most prior field studies of new particle formation (NPF) have been performed at or near ground level, leaving many unanswered questions regarding the vertical extent of NPF. To address this, we measured concentrations of 11–16 nm diameter particles from ground level to 1000 m during the 2013 New Particle Formation Study at the Atmospheric Radiation Measurement Southern Great Plains site in Lamont, Oklahoma. The measurements were performed using a tethered balloon carrying two condensation particle counters that were configured for two different particle cut-off diameters. These observations were compared to data from three scanning mobility particle sizers at the ground level. We observed that 11–16 nm diameter particles were generated at the top region of the boundary layer, and were then rapidly mixed throughout the boundary layer. We also estimate liquid water content of nanoparticles using ground-based measurements of particle hygroscopicity obtained with a Humidified Tandem Differential Mobility Analyzer and vertically resolved relative humidity (RH) and temperature measured with a Raman lidar. Our analyses of these observations lead to the following conclusions regarding nanoparticles formed during NPF events at this site: (1) ground-based observations may not always accurately represent the timing, distribution, and meteorological conditions associated with the onset of NPF; (2) nanoparticles are highly hygroscopic and typically contain up to 50 % water by volume, and during conditions of high RH combined with high particle hygroscopicity, particles can be up to 95 % water by volume; (3) increased liquid water content of nanoparticles at high RH greatly enhances the partitioning of water-soluble species like organic acids into ambient nanoparticles.

1 Introduction

New particle formation (NPF) and growth are frequently observed in the atmosphere worldwide (Finlayson-Pitts and Pitts Jr., 2000; Kulmala et al., 2004; Seinfeld and Pandis, 2006; Zhang et al., 2011). One of the most important potential impacts of NPF is the creation of cloud condensation nuclei (CCN), which can modify cloud properties and thereby affect climate and precipitation (Kerminen et al., 2005; Pierce and Adams, 2007; Spracklen et al., 2008; Kuang et al., 2009; Merikanto et al., 2009; Pierce and Adams, 2009; Pierce et al., 2012; Westervelt et al., 2013; Farmer et al., 2015). Sulfuric acid is often associated with the formation and growth of new particles (Weber et al., 1996, 1997, 2001; Stolzenburg et al., 2005; Kuang et al., 2008; Sipilä et al., 2010; Kulmala et al., 2013), but other species such as methanesulfonic acid (Kreidenweis and Seinfeld, 1988; Kreidenweis et al., 1989; Wyslouzil et al., 1991a, b; Dawson

et al., 2012; Chen et al., 2015b), ammonia (Korhonen et al., 1999; Benson et al., 2009; Kirkby et al., 2011; Zollner et al., 2012), amines (Kurtén et al., 2008; Smith et al., 2010; Berndt et al., 2010; Erupe et al., 2011; Zollner et al., 2012; Yu et al., 2012; Almeida et al., 2013; Glasoe et al., 2015), and highly oxidized organic species (Zhang et al., 2004; Riipinen et al., 2011; Ehn et al., 2012; Zhao et al., 2013; Donahue et al., 2013; Kulmala et al., 2013; Riccobono et al., 2014) also play a role. Many observations of NPF have been performed on the ground (Kulmala et al., 2004), but some measurements suggest that nucleation can be altitude-dependent (Weber et al., 1999; Lee et al., 2003). Colder temperatures and higher relative humidity (RH) at higher altitudes may favor the binary nucleation of H_2SO_4 and H_2O, but at lower altitudes bases can play a substantial role due to the closer proximity to surface sources of these precursors (Weber et al., 1999). Ion-induced particle formation is suggested to be important in the upper troposphere and lower stratosphere due to the stronger intergalactic cosmic rays that generate ions in these regions (Lee et al., 2003; Dunne et al., 2016). Vertically resolved measurements of NPF are therefore needed to better understand the species involved in NPF and the underlying mechanisms, as well as adequately assess the impacts of NPF on cloud formation and climate.

Only a few studies have focused on the vertical extent of new particle formation. During the SATURN ("Strahlung, vertikaler Austausch, Turbulenz und Partikel-Neubildung", or "Radiation, Vertical Exchange, Turbulence and New Particle Formation") campaign in Germany, tethered balloon-borne measurements were performed to obtain vertical profiles of SO_2 concentration, particle number concentration, and meteorological parameters together with ground-based measurements (Stratmann et al., 2003; Siebert et al., 2004; Wehner et al., 2007). The group observed two NPF events on the same day. The first one was initiated in the residual layer before the breakup of the thermal inversion layer, and those newly formed particles were then mixed down during the subsequent breakup process. The second NPF event occurred in the entire well mixed layer during and after the breakup process of the thermal inversion layer. New particle formation can also be initiated near the top of the inversion layer due to intensive mixing caused by plumes penetrating the inversion (Siebert et al., 2004), and within a thin layer around 200 m above the ground (Wehner et al., 2007). Laakso et al. (2007) also observed NPF in the mixed boundary layer and free troposphere in southern Finland using measurements on board a hot air balloon. The rapid downward mixing of small aerosol particles from the free troposphere represents an important source of aerosol particles in the pristine Amazon boundary layer (Wang et al., 2016; Andreae et al., 2017). Helicopter (Kupiszewski et al., 2013) and aircraft (Burkart et al., 2017) measurements of vertical profiles of aerosol particles in the summertime Arctic observed particle formation in the near-surface layer, with much lower concentrations at higher altitudes.

The ability for a nanoparticle formed by NPF to grow to CCN size is dependent on its growth rate in relation to the rate of loss due to coagulational scavenging (McMurry and Friedlander, 1979; Kerminen and Kulmala, 2002; Kuang et al., 2009; Westervelt et al., 2013; Pierce et al., 2014). There has been much attention paid to understanding growth rates of newly formed particles. Thus far, mechanisms of new particle growth such as salt formation (Barsanti et al., 2009; Smith et al., 2010; Hodshire et al., 2016), condensation of extremely low-volatility organic compounds (ELVOCs) (Riipinen et al., 2011; Donahue et al., 2011; Riipinen et al., 2012; Jokinen et al., 2012; Ehn et al., 2014; Hodshire et al., 2016; Pierce et al., 2011), and reactive uptake of organics through particle-phase reactions such as aldol condensation (Jang et al., 2002; Limbeck et al., 2003; Barsanti and Pankow, 2004), have been identified. Many of these reactions in newly formed particles might be enhanced by high water content, which has been shown for submicron particles in many field, laboratory, and modeling studies (Blando and Turpin, 2000; Hennigan et al., 2008; Galloway et al., 2009; Ervens et al., 2011; Carlton and Turpin, 2013). In addition, the enhancing effect of water in NPF and growth was observed in the reaction of methanesulfonic acid and amines (Chen et al., 2015a, b). While many field and laboratory measurements over the past several decades have quantified water uptake of submicron-size particles, very little is known about the water content of newly formed particles, especially how it responds to relative humidity that is vertically and temporally variable in the atmosphere.

This paper describes vertical profile measurements of 11–16 nm diameter atmospheric aerosol particles from a tethered balloon during the New Particle Formation Study at the Department of Energy (DOE) Atmospheric Radiation Measurement (ARM) Southern Great Plains (SGP) research site in Lamont, Oklahoma. Those observations were supplemented by simultaneous ground-based measurements of particle number size distributions and size-resolved particle hygroscopicity. We explore the use of Raman lidar measurements of vertically and temporally resolved temperature and relative humidity to provide insights into the range of liquid water content for newly formed particles. The effect of liquid water content of newly formed particles on particle growth is examined by a growth model. The goals of this study are to (1) fully characterize the time and location of new particle formation events at this site, and (2) provide insights into the liquid water content of newly formed particles and their potential to undergo aqueous reactions and/or activate into cloud droplets.

2 Methods

2.1 Measurements

Vertical profiles of 11–16 nm diameter particles were measured as part of the 2013 SGP New Particle Formation Study (NPFS) (Hodshire et al., 2016; NPFS, 2017). NPFS was sponsored by the US Department of Energy with participation from the University of Delaware, University of Minnesota, Augsburg College, and the National Center for Atmospheric Research (NCAR). This field study addressed the formation and growth of particles as well as the impacts of newly formed particles on cloud processes. NPFS took place at the Central Facility of the SGP site, spanning the dates of 13 April–24 May 2013. The site is representative of the large Great Plains region, and characterized by active agricultural activities, as well as oil extraction and refineries. During the study, 13 NPF events were observed. Guest instruments that are relevant to the current study include three ground-based scanning mobility particle sizers (SMPSs) to measure the particle size distribution from 1.9 to 528 nm, and two handheld condensation particle counters (CPCs) for particle number concentration measurements deployed on a tethered balloon (TBSNPFS, 2017). Both the SMPSs and the CPCs measured particles under ambient conditions.

Three SMPSs were operated in parallel on the ground, including a DEG SMPS (a TSI 3085 nano-differential mobility analyzer coupled with a diethylene glycol-based condensation particle counter; 1.9–13.9 nm mobility diameter) (Jiang et al., 2011), a nano-SMPS (a TSI 3085 nano-differential mobility analyzer coupled with a TSI 3025A particle counter; 2.8–47 nm mobility diameter), and a conventional SMPS (a home-built long column differential mobility analyzer, similar in design to a TSI 3071, coupled with a TSI 3760 CPC; 23–528 nm mobility diameter). While measurements overlapped, the data were merged to provide the best estimate of the correct size distribution.

The tethered balloon was a helium-filled blimp-shaped balloon made by Blimpworks (Statesville, NC, USA), owned and operated by NCAR (Greenberg et al., 1999, 2014). The balloon was 6.4 m long, ∼ 1.5 m in diameter at the widest point, and had a filled volume of 12 m^3. The height of the balloon was controlled by an NCAR-built winch with circuitry that provides a user-defined constant rate of altitude change. Two handheld condensation particle counters (CPCs; TSI 3007) were mounted under the balloon, each adjusted to a different diameter cut-off point. This enabled the ability to count particles between 11 and 16 nm by taking the difference in the two measurements. A small weather meter was used to log altitude (pressure), temperature, and wind speed. Details of this payload are provided below.

The CPCs allow detection of particles by exposing the sampled aerosol to a warm saturated alcohol vapor. This flow is then cooled using a thermal electric device (TED), causing the alcohol vapor to condense onto particles and grow particles to micron-sized droplets that can be detected by light scattering. The voltage applied to the TED directly affects the temperature difference between the saturated and condenser regions within the CPC, which in turn defines size-dependent detection efficiencies as shown in Fig. 1 for TED voltages of 1600 and 1000 mV. The cut-off sizes (defined as the size at which particles are detected with 50 % efficiency) are about 11 nm and 16 nm for the CPCs, with TEDs operating at 1600 and 1000 mV, respectively. The number concentration of particles in the size range of 11–16 nm ($N_{11–16}$) was estimated by subtracting measurements from the two CPCs. The time resolution of CPC measurements is 1 s, and the uncertainty is ±20 %.

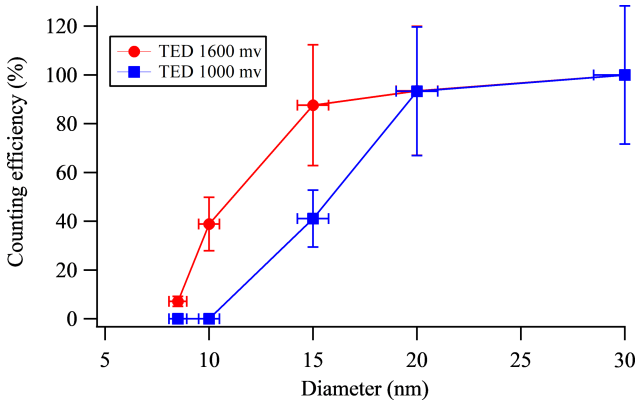

Figure 1. Counting efficiency as a function of particle diameter is shown for two TSI 3007 CPCs. Thermal electric devices (TEDs) of the two CPCs were set at 1000 and 1600 mV, respectively. The counting efficiencies were calculated relative to counts with thermal electric device set at 2000 mV for atomized ammonium sulfate particles. Uncertainty in diameter is ±5 %, estimated from the uncertainties in the voltage and flow conditions in the DMA used for calibration. Uncertainty in ratio is ±28 %, and is calculated using the published concentration accuracy of the model 3007 CPCs (±20 %).

A battery-powered handheld meteorological gauge (Kestrel 4500, Nielsen-Kellerman Co.) was attached to the tethered balloon, approximately 0.2 m above the CPCs, which were ∼ 0.5 m below the bottom of the balloon. Since the balloon always points into the wind, the wind direction measurements were obtained by the compass feature. Other meteorological parameters such as altitude, wind speed, RH, and temperature were also recorded by the gauge.

Launches were made during daylight hours. The balloon was raised and lowered at a constant rate of 0.5 m s^{-1}, and reached a maximum altitude of 800–1200 m above ground level. One launch, defined as one cycle of raising and lowering the balloon, took place over a minimum time of ∼ 46 min. During periods of continuous sampling, we repeated launches every ∼ 60 min, which allowed for a brief break period for the operators to replace batteries, assess data quality, and perform any other required maintenance. Four

days were studied with the tethered balloon: 12, 13, 16, and 17 May 2013. The day of 12 May 2013 corresponded to a NPF event. The day of 13 May 2013 was an intermittent NPF day, on which the growth of new particles was interrupted by the change of wind direction. The other 2 days were non-event days, and are not discussed in this paper.

In addition to guest instruments provided by NPFS participants, the SGP site was equipped with a variety of instruments for probing atmospheric structure and properties, as well as physicochemical properties of trace gases and particles (NPFS, 2017). Instruments relevant to the current study include a Tandem Differential Mobility Analyzer (TDMA) (Collins, 2010) to measure size-resolved hygroscopicity of particles, Doppler lidar (Newsom, 2012) to measure vertical wind velocity, and Raman lidar (Turner, 2009) to measure vertical profiles of RH and temperature. The planetary boundary layer (PBL) heights were obtained from the ARM value-added product that determines PBL height with radiosonde measurements based on the profile of the bulk Richardson number (Sivaraman et al., 2013). The radiosonde measurements were performed at 05:00, 11:00, 17:00, and 23:00 UTC (00:00, 06:00, 12:00, and 18:00 local time) each day, resulting in four PBL heights at their corresponding times. Linear interpolation of two consecutive measurements was used to estimate the evolution of PBL.

2.2 Estimates of hygroscopicity parameter, water content of nanoparticles, and atmospheric stability

The TDMA system consists of two high-flow differential mobility analyzers (Aerosol Dynamics, Inc.), a charger, two Nafion tubes, and a CPC (Collins, 2010). The air sample was first dried in a Nafion tube, and then drawn through a charger before entering the first differential mobility analyzer. The voltage applied to the first differential mobility analyzer was fixed to produce a mono-mobility aerosol of known particle mobility diameter. The monodisperse aerosol was then introduced into the second Nafion tube to elevate RH to 90 %, and the growth of the monodisperse aerosol was characterized by the second differential mobility analyzer with a CPC. A typical measurement sequence required roughly 45 min. The TDMA was calibrated every night shortly after midnight by injecting a polydispersed, pure ammonium sulfate aerosol that has a known hygroscopicity.

The TDMA system provides size-resolved normalized distribution of hygroscopic growth factor (f_i), which is defined as the ratio of the hydrated particle diameter at RH 90 % to the dry diameter, throughout a day. The hygroscopic growth factors for particles with diameters of 13, 25, 50, 100, and 200 nm are used for analysis in this study. The hygroscopicity parameter κ for a certain size of particles at the corresponding time of a day can be calculated by (Kreidenweis et al., 2008; Petters and Kreidenweis, 2007)

$$\kappa = \sum \varepsilon_i \kappa_i = \sum \varepsilon_i \left(f_i^3 - 1\right)\left[\left(\exp\left(\frac{4\sigma_{s/a} M_w}{RT\rho_w D_{dry} f_i}\right)/\mathrm{RH}\right) - 1\right], \quad (1)$$

where ε_i is the normalized fraction of aerosol with a hygroscopic diameter growth factor (f_i), $\sigma_{s/a}$ is the surface tension of the solution–air interface and is assumed to be the same as the surface tension of water, 0.072 J m^{-2}, M_w is the molecular weight of water, R is the universal gas constant, T is the temperature during the TDMA measurements and is assumed to be 298.15 K, ρ_w is the density of water, D_{dry} is the diameter of the dry particles, and RH is the relative humidity (0.9).

Since vertical profiles of RH and temperature profiles are available from Raman lidar measurements, we combine these data with TDMA-derived measurements of κ to estimate the profile of water content of newly formed particles. The growth factor (f) and water volume ratio (ϕ) of particles at elevated heights within the boundary layer can be estimated using Eqs. (2) and (3) (Petters and Kreidenweis, 2007; Kreidenweis et al., 2008), assuming that the boundary layer is well mixed so that particles at elevated heights have the same κ as particles measured at ground level:

$$\mathrm{RH} = \frac{f^3 - 1}{f^3 - (1-\kappa)} \exp\left(\frac{4\sigma_{s/a} M_w}{RT\rho_w D_{dry} f}\right) \quad (2)$$

$$\phi = \frac{V_{wet}}{V_{dry}} = f^3, \quad (3)$$

where T and RH are the temperature and relative humidity at the selected time and height obtained from Raman lidar measurements, V_{wet} is the volume of the wet particle, and V_{dry} is the volume of the dry particle. The growth factor f was obtained by solving the cubic Eq. (2) in the physically meaningful range of $f > 1$. Supersaturation of more than 1–2 % relative to water is rarely seen in the atmosphere due to the prevalent existence of CCN (Rogers and Yau, 1989). Therefore, data with RH > 101 % were treated as systematic errors and neglected from analysis. When RH is between 100 and 101 %, there are two solutions to Eq. (2), but only the lower one is at a stable state. When RH is lower than 100 %, there is only one solution of f for $f > 1$ (Seinfeld and Pandis, 2006; Petters and Kreidenweis, 2007).

While the surface tension of water, 0.072 J m^{-2}, was used in Eqs. (1) and (2), atmospheric particles are known to contain some surface active compounds (Facchini et al., 1999; Svenningsson et al., 2006). The presence of surface active compounds in particles can suppress surface tension to a significant extent. Therefore, sensitivity studies were carried out by decreasing $\sigma_{s/a}$ used in Eqs. (1) and (2) to examine its effects on estimated κ values and water volume ratios of particles.

In order to determine the stability of the boundary layer, the Richardson number (R_i) was calculated using Eq. (4) (Woodward, 2010):

$$R_i(z_1) = \frac{g}{T(z_1)} \frac{\left[\frac{T(z_1)-T(z_2)}{z_1-z_2}\right]}{\left[\frac{u(z_1)-u(z_2)}{z_1-z_2}\right]^2}, \quad (4)$$

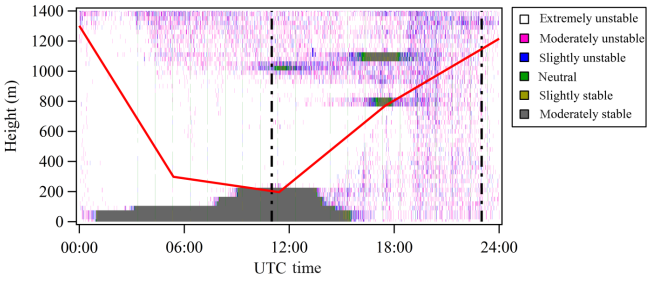

Figure 2. Vertically and temporally resolved atmospheric stability on 12 May 2013 at SGP. The atmospheric stability is classified into extremely unstable (white), moderately unstable (magenta), slightly unstable (blue), neutral (green), slightly stable (brown), and moderately stable (grey) regimes based on Richardson number. The two vertical dashed lines represent 06:00 and 18:00 local time, respectively. The red line shows the boundary layer height determined from radiosonde data.

where z is the height, g is the gravitational acceleration, T is the ambient temperature at the reference height obtained from Raman lidar measurements, and u is the vertical wind speed at the reference height obtained from Doppler lidar measurements. Based on the Richardson number, the stability of the boundary layer can be classified into six Pasquill stability regimes: A – extremely unstable; B – moderately unstable; C – slightly unstable; D – neutral; E – slightly stable; and F – moderately stable.

The atmospheric stability within the boundary layer on 12 May 2013 during the campaign is shown in Fig. 2. Data herein are provided in UTC time, which is 5 h ahead of the local time during the campaign. Plots showing the atmospheric stability of other selected days of interest are included in Fig. S1 in the Supplement. The boundary layer was moderately stable at night, suggesting that a thermal inversion layer developed at night and suppressed convection. The boundary layer was under extremely or moderately unstable conditions during the daytime because the thermal inversion layer dissipated and eventually disappeared after sunrise. Given that NPF events in this study occurred during the daytime, a well mixed boundary layer is a reasonable assumption. While a well mixed boundary layer makes it likely that particles measured at ground level are representative of those aloft, it does not guarantee it. This should be borne in mind in the subsequent discussion.

2.3 Model description

In order to explore the effect of increasing relative humidity on the relative uptake of each chemical species into particles, the particle growth model MABNAG (Model for Acid-Base chemistry in NAnoparticle Growth) is used to model the NPF events observed on the case days of 19 April, 9 May, and 11 May over a relative humidity range of 30–95 % in 5 % increments. These days were selected because extensive measurements of particle composition and gas-phase species were performed; these observations were presented in detail in Hodshire et al. (2016). Each day featured with different dominant species contributing to particle growth: 19 April was from ELVOCs, 9 May was from inorganic salts like ammonium sulfate, and 11 May was from ELVOCs, amines/ammonia, and sulfate. MABNAG, developed by Yli-Juuti et al. (2013), simulates the growth and composition of a single particle as it undergoes condensation of low-volatility vapors and acid-base reactions in the particle phase. The version of MABNAG used in this study accepts as inputs the gas-phase concentrations and properties (molar mass, pKa, vapor pressure, and Henry's law constant or diffusion coefficient) of water, sulfuric acid, a single organic acid (to be representative of organic acids in general), ammonia, a single amine (chosen to be representative of amines in general), and a non-reactive organic compound, assumed here to be an ELVOC. Malonic acid and dimethylamine (DMA) were selected as the representative organic acid and base, respectively, in this study. The initial particle is assumed to be made of 20 molecules of each input species, creating a particle that is approximately 3 nm in diameter. The particle density is assumed to be species-independent and is set to 1.5 g cm^{-3}; the particle surface tension is set to 0.03 J m^{-2}. MABNAG calculates the uptake rates of sulfuric acid, the organic acid, and the ELVOC species as gas-phase diffusion-limited mass transfer as functions of their ambient vapor pressures, equilibrium vapor pressures, and gas-phase diffusivities. Water and the base species are assumed to reach instantaneous equilibrium between gas and particle phases. Upon uptake, particle-phase acid dissociation and base protonation are calculated by the Extended Aerosol Inorganics Model (E-AIM, 2017) (Clegg et al., 1992; Wexler and Clegg, 2002; Clegg and Seinfeld, 2006a, b). The ELVOC is not allowed to dissociate in the particle phase, and is assumed to undergo irreversible condensation due to its low vapor pressure.

As discussed in Hodshire et al. (2016), there are limitations and uncertainties to many of the MABNAG inputs. MABNAG can only accept the chemical properties of one organic acid and one amine, although both oxalic and malonic acid were measured and many different amines were observed. Further, there are uncertainties in the measured oxalic acid concentration, the vapor pressures of the organic acids, and whether or not the larger amines (containing at least four carbons) participate in particle growth. For simplicity, we model only the base case from Hodshire et al. (2016) over the given relative humidity range (30–95 %). This base case assumes the organic acid properties of malonic acid, the equilibrium vapor pressure for malonic acid to be that as reported in Bilde et al. (2015), the organic acid concentration to be that of the sum of the measured malonic acid and 10 times the measured oxalic acid concentration (due to a likely low bias of the oxalic acid measurements), the amine chemical properties of DMA, and the amine concentration to be the sum of the measured methylamine, DMA, and trimethylamine only.

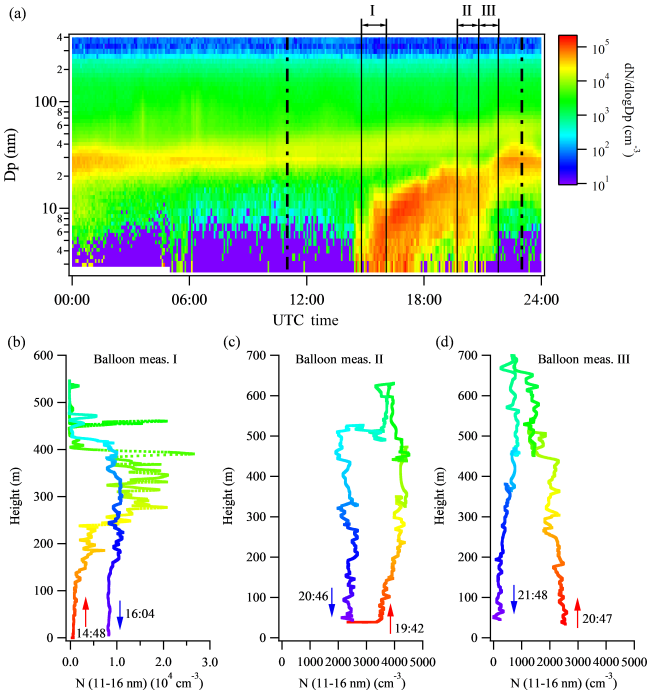

Figure 3. New particle formation event on 12 May 2013 at SGP. **(a)** Particle size distributions captured by ground-based scanning mobility particle sizers. The two vertical dashed lines represent 06:00 and 18:00 local time, respectively. The vertical black solid lines represent the time frames of the tethered balloon measurements. **(b–d)** Vertical profiles of particle number concentration in the size range of 11–16 nm measured by the tethered balloon system. Three launches were made during the new particle formation event. A rainbow color pattern is used to illustrate the time after the balloon measurements were started, with red representing the initial period and purple representing the final period of a launch.

A more detailed description of the inputs used for this study and the conditions of the three case days can be found in Hodshire et al. (2016).

3 Results and discussion

3.1 Vertical profiles of particle number concentration in the size range of 11–16 nm in relation to ground-based measurements of number-size distribution

Figure 3 shows the NPF event on 12 May 2013 at the ARM SGP site as captured by the ground-based SMPS and tethered balloon system. A burst of small particles appeared approximately at 15:00 UTC (10:00 local time), and they continually grew to ∼ 30 nm within the next several hours (Fig. 3a). The tethered balloon was launched three times on this day, and the corresponding vertical profiles of particle number concentration in the size range of 11–16 nm ($N_{11\text{-}16}$) are shown in Fig. 3b–d. The vertical profiles of RH and temperature are

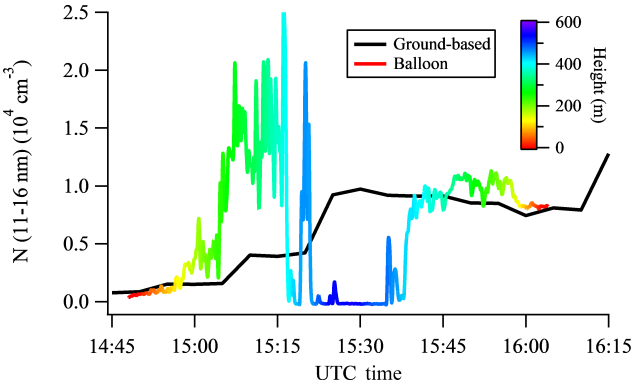

Figure 4. Time evolution of particle number concentrations in the size range of 11–16 nm at SGP during the initial period of new particle formation on 12 May 2013 obtained by the ground-based ground-based scanning mobility particle sizers and tethered balloon system.

shown in Fig. S2. For the first ascent starting at 14:48 UTC (Fig. 3b), $N_{11\text{–}16}$ is negligible within the lowest 100 m, and increases gradually as the balloon raised up to ∼ 100 m. Maximum values of up to 2.0×10^4 cm^{-3} were observed at 300–400 m. $N_{11\text{–}16}$ is almost zero as the balloon reached up to ∼ 400 m. During the subsequent descent, $N_{11\text{–}16}$ is relatively constant at $\sim 1.0 \times 10^4$ cm^{-3}, and shows little variation with height. The vertical profile of temperature (Fig. S2a) shows a lapse rate between 0.9 and 1.2 °C per 100 m up to ∼ 400 m. The profile of relative humidity (Fig. S2a) features some fluctuations between 45 and 55 % at the lowest 400 m but a rapid decrease at 400 m, at the same height where a small increase of temperature and a sharp decrease of $N_{11\text{–}16}$ were observed. These together indicate that during the first launch of the tethered balloon, the mixed layer had a height of about 400 m.

Compared to the first launch, the values of $N_{11\text{–}16}$ for the second and third launches are lower (Fig. 3c–d). From the second ascent starting at 19:42 UTC to the third descent ending at 21:48 UTC, $N_{11\text{–}16}$ keeps decreasing with time, and does not exhibit any sharp fluctuation with height. The vertical profiles of temperature and RH for the two launches are similar, showing a temperature lapse rate between 0.9 and 1.0 °C per 100 m, and increasing RH with height.

To further compare ground-based and balloon-borne measurements, particle number concentrations in the size range of 11–16 nm measured by the ground-based SMPS during the first launch were integrated by taking into account the slopes of the detection efficiency curves of the two balloon-borne CPCs. The result is shown in Fig. 4. During the ascent, $N_{11\text{–}16}$ measured aloft is up to 10-fold larger than that measured by the ground-based SMPS, while $N_{11\text{–}16}$ measured by the two systems agrees reasonably well during the subsequent descent of the balloon. The ground-based SMPS together with the balloon-borne measurements suggest that new particle formation was initiated at the top region of

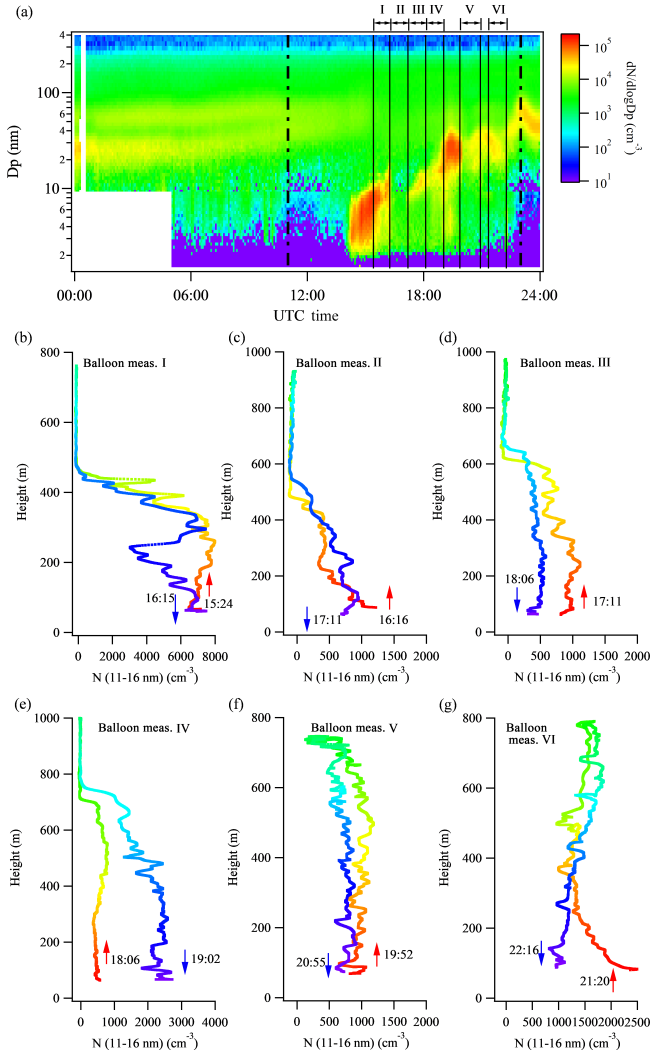

Figure 5. New particle formation event on 13 May 2013 at SGP. **(a)** Particle size distributions captured by ground-based scanning mobility particle sizers. The two vertical dashed lines represent 06:00 and 18:00 local time, respectively. The vertical black solid lines represent the time frame of the tethered balloon measurements. **(b–g)** Vertical profiles of particle number concentration in the size range of 11–16 nm measured by the tethered balloon system. Six launches were made during the new particle formation event. A rainbow color pattern is used to illustrate the time after the balloon measurements were started, with red representing the initial period and purple representing the final period of a launch.

the boundary layer, and subsequently mixed downward to ground level due to the unstable conditions and therefore the strong vertical mixing within the boundary layer (Fig. 2).

Similar measurements were made during an interrupted NPF day of 13 May 2013 (Fig. 5). A burst of small particles appeared at 14:00 UTC at the ground level, and continually grew to ∼ 10 nm before being interrupted by the change of wind direction from southwest (180–220°) to northwest (270–310°) at about 16:00 UTC (Fig. 5a). The growth of newly formed particles was observed after the wind direction changed back to southwest at about 19:00 UTC. Some shorter interruptions followed in the late afternoon (20:00–23:00 UTC). Six balloon launches were made on this day, and the corresponding vertical profiles of $N_{11–16}$ as well as temperature and RH are shown in Figs. 5b–g and S3, respectively. Since the initial period of the NPF event was not captured by the tethered balloon system, it is not known whether the NPF was initiated aloft or at the ground level. However, similar to the NPF event on 12 May, the entire boundary layer appeared to be well mixed with $N_{11–16}$ within about 1 h after NPF was first observed on the ground.

The comparison of ground-based and balloon-borne measurements for the 2 days provides insights into the vertical extent of NPF and the vertical mixing process within the boundary layer. The NPF event on 12 May was initiated at the top region of the boundary layer followed by a rapid downward mixing process. The timescale of the vertical mixing was approximately 0.5–1 h. Although the background concentration of particles before NPF was not captured by the tethered balloon system on 13 May, the boundary layer appeared to be well mixed with ultrafine particles, suggesting a strong vertical mixing on this day. Implicit in these statements is that the vertical distribution of NPF is adequately represented by the vertical distribution of 11–16 nm diameter particles. Particle formation is estimated to have been initiated 3–4 h prior to detection by the balloon-borne CPCs, based on the ∼ 3 nm h^{-1} diameter growth rate of the 12 May event as determined from the size distributions shown in Fig. 3a. Because of this, there is some degree of uncertainty associated with linking these observations to NPF. Deploying CPCs that are lightweight, low-powered, and can detect sub-3 nm diameter particles can eliminate this uncertainty. Such particle counters do not exist currently, but rapid progress is being made in this area.

3.2 Size-resolved hygroscopicity of particles

Size-resolved 1 h average values of the hygroscopicity parameter, κ, for the whole campaign are shown in Fig. 6. The κ values of 13 nm particles ($\kappa_{13\,nm}$) are in the range of 0.5–0.9, significantly larger than those of larger size particles, and exhibit a distinct diurnal pattern of increasing in the daytime and decreasing at night. The values of $\kappa_{25\,nm}$ are in the range of 0.1–0.3, much smaller than $\kappa_{13\,nm}$ but slightly larger than those of larger size particles. The κ values of larger size particles are similar, and do not show a distinct diurnal pattern. While κ values in Fig. 6 were calculated assuming that the surface tension of the solution–air interface is the

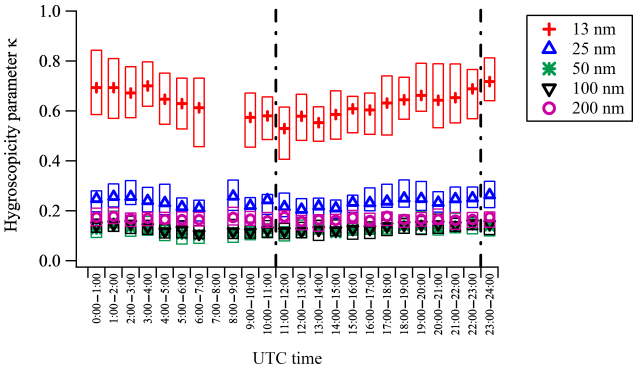

Figure 6. One-hour average hygroscopicity parameters κ for 13, 25, 50, 100, and 200 nm particles determined by TDMA from 13 April to 24 May 2013 at SGP. The boxes represent 25–75 % ranges of all measurements. The two vertical dashed lines represent 06:00 and 18:00 local time, respectively.

same as water (0.072 J m^{-2}), a sensitivity analysis was carried out by decreasing $\sigma_{s/a}$ by 30 % (0.0504 J m^{-2}) or using $\sigma_{s/a}$ as the one used in the MABNAG model (0.03 J m^{-2}). The size-resolved hygroscopicity parameter, κ, calculated using lower values of surface tension, shows a similar pattern (Fig. S4), indicating that uncertainties in surface tension of the solution–air interface do not affect the discussion here.

The hygroscopicity of particles is strongly dependent on their chemical composition. Particles composed of inorganic salts, acids, and highly oxidized organic species grow significantly in response to increased RH, while particles containing less oxidized organic species, soot, and dust exhibit little hygroscopic growth. Values of κ are in the range of 0.5–1.4 for atmospherically relevant salts and small acids, and 0.01–0.5 for slightly to very hygroscopic organic species (Petters and Kreidenweis, 2007). The growth factor of nanoparticles of the same chemical composition decreases with size due to the Kelvin effect (Hämeri et al., 2000, 2001; Park et al., 2009; Lewis, 2006). The higher κ values of 13 nm particles observed at the SGP site suggest that they contained a larger fraction of highly hygroscopic species such as inorganic salts, acids, and highly oxidized organic compounds. Gaseous precursors of those highly hygroscopic species might be formed photochemically (e.g., oxidation of SO_2 to form H_2SO_4, oxidation of volatile organic compounds to form ELVOCs), or might be enhanced due to higher emissions at elevated daytime temperatures (e.g., emission of NH_3 and amines from soil and animal husbandry), resulting in the distinct diurnal variation of $\kappa_{13\,nm}$. As particles grew larger, less oxidized organic species contributed to particle growth, leading to lower values of κ.

3.3 Estimates of vertically resolved nanoparticle liquid water content

While ultrafine particles are highly hygroscopic, and can be formed aloft as discussed earlier, the profiles of water volume ratio of 13 nm particles were estimated based on the RH and temperature profiles obtained from Raman lidar measurements, assuming that $\kappa_{13\,nm}$ is representative of 13 nm particles throughout the boundary layer. This assumption is supported by the observation of the extremely unstable boundary layer during the daytime based on the Richardson number analysis (Figs. 2, S1). The profiles of estimated water volume ratio for 13 nm particles on 12 and 13 May 2013 are shown in Fig. 7. Also shown in Fig. 7 are temporally resolved $\kappa_{13\,nm}$ obtained by TDMA and the RH (open black circles in upper plots) and temperature (white contour lines in the lower plot) profiles of ambient air on these days. Consistent with the tethered balloon measurements (Figs. S2, S3), relative humidity is in the range of 30–60 %, and is higher at the top of the boundary layer after 18:00 UTC. The increased RH is possibly due to increasing boundary layer depth and lower temperature at higher altitude (Ek and Mahrt, 1994). Temperature decreases with increased height in accord with tethered balloon measurements. The $\kappa_{13\,nm}$ values show an increasing trend as NPF was initiated on 12 and 13 May 2013, suggesting that highly hygroscopic species were involved in NPF and subsequent growth. The water volume ratios (ϕ) of 13 nm particles are highly variable depending on RH, temperature, and κ, and were estimated to be in the range of 1–2.

It is noteworthy that $\sigma_{s/a}$ can be smaller than the surface tension of water, 0.072 J m^{-2}, if surface-active compounds were present as discussed earlier. A sensitivity study was carried out by decreasing $\sigma_{s/a}$ used in Eqs. (1) and (2) to 0.0504 and 0.03 J m^{-2} to examine its effects on κ values and estimated water volume ratios of particles. Using 30 and 58 % lower values of $\sigma_{s/a}$ results in $\sim$ 17 and $\sim$ 30 % lower values of κ, respectively (Fig. S5). However, these lower κ values were applied in Eq. (2) along with the lower $\sigma_{s/a}$ to predict the particle growth factor. Since κ and $\sigma_{s/a}$ were applied self-consistently in Eqs. (1) and (2), water volume ratios of particles estimated with 30 and 58 % lower values of $\sigma_{s/a}$ are only $\sim$ 2 and $\sim$ 4 % higher, respectively, suggesting that uncertainties in $\sigma_{s/a}$ have a relatively minor effect in estimates of water volume ratio of particles.

There are other uncertainties in estimating the water content of 13 nm particles. First, although the boundary layer appeared to be well mixed based on the Richardson number, the hygroscopicity parameter κ of 13 nm particles measured at the ground level might be not representative of κ throughout the entire boundary layer. Figure S6 shows how water volume ratio of 13 nm particles varies with κ and RH at 298.15 K. While $\kappa_{13\,nm}$ was not measured at elevated heights, the variation of $\kappa_{13\,nm}$ measured at the ground, 0.5–0.9 (Fig. 6), is used to evaluate uncertainties of estimated water ratio here. Decreasing $\kappa_{13\,nm}$ from 0.9 to 0.5 results in

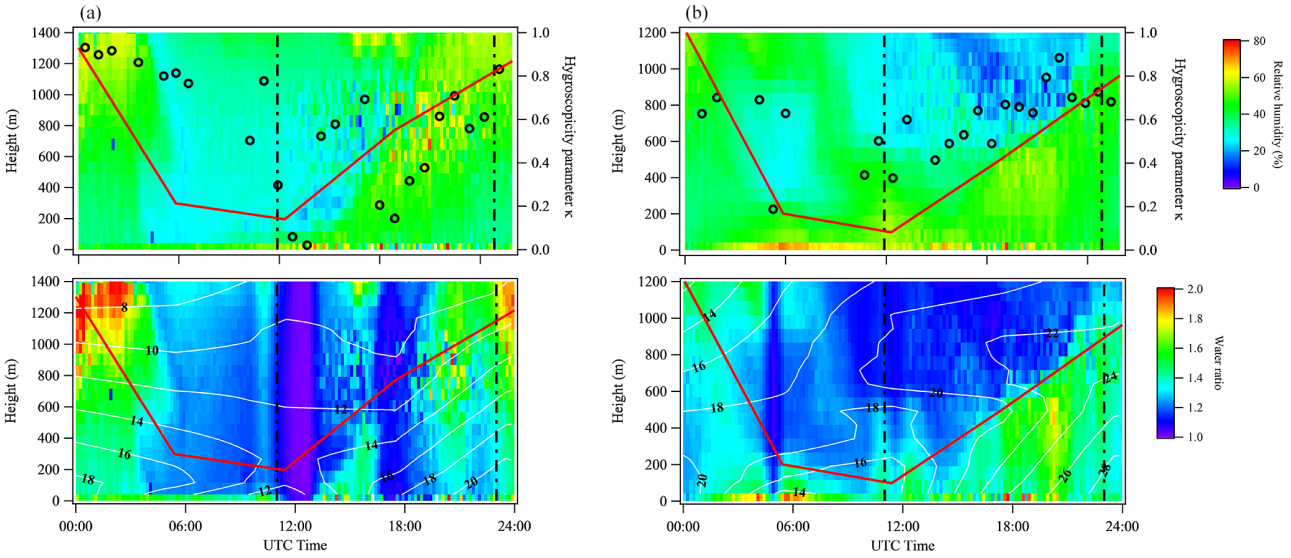

Figure 7. Vertically and temporally resolved relative humidity (upper plot) and estimated water volume ratio of 13 nm particles (lower plot) at SGP on **(a)** 12 May 2013 and **(b)** 13 May 2013. The two vertical dashed lines in each plot represent 06:00 and 18:00 local time, respectively. The red line shows the boundary layer height determined from radiosonde data. Overlaid in the upper plot is the temporally resolved hygroscopicity parameter κ of 13 nm particles obtained by TDMA (open black circles). Temperature (°C) is shown by the white contour lines in the lower plot.

a decrease of water volume ratio of 13 nm particles from 1.53 to 1.29 at RH 40 %, and from 2.16 to 1.63 at RH 60 %. This suggests that even if $\kappa_{13\,\mathrm{nm}}$ at elevated heights is relatively low, particles can still have significant water content in ambient air. Second, κ is defined through its effect on the water activity of the solution. While κ was assumed to be independent of RH, the change of water activity with RH can lead to a non-constant κ value over the range of RH, but the effect was suggested to be minimal (Petters and Kreidenweis, 2007).

In addition to the 2 days during which tethered balloon measurements were carried out, another three NPF events that featured three distinct growth pathways, and were discussed by Hodshire et al. (2016), were selected to estimate the profiles of water volume ratio. Figure 8 shows observations from 9 May 2013, during which particle growth was mainly driven by sulfuric acid and ammonia, with small but nontrivial contributions from organics and amines (Hodshire et al., 2016). The $\kappa_{13\,\mathrm{nm}}$ value increases significantly to up to ~ 1 as NPF started. The high value of $\kappa_{13\,\mathrm{nm}}$ is consistent with sulfuric acid and ammonia as the main species contributing to NPF and growth. Relative humidity is in the range of 60–101 %, and is significantly higher than that for the 2 days with tethered balloon measurements (Fig. 7). Because of the high $\kappa_{13\,\mathrm{nm}}$ and RH, estimated water volume ratios of 13 nm particles are substantially higher, and can reach to ~ 18 at the top of the boundary layer.

For the day of 19 April 2013 (Fig. S7), on which particles grew mainly by acid-base reactions of organic acids and amines and/or irreversible condensation of ELVOCs, the $\kappa_{13\,\mathrm{nm}}$ value stays constant at ~ 0.6 in the period of NPF and growth, and estimated water volume ratios of 13 nm particles are in the range of 1–3. For the day of 11 May 2013 (Fig. S8), on which sulfate, organics, and bases are important for growth, an increase of $\kappa_{13\,\mathrm{nm}}$ was observed as NPF started. The estimated water volume ratios of 13 nm particles during the day are in the range of 1–3. Our estimates of water volume ratios of 13 nm particles for 5 different NPF days suggest that newly formed particles were highly hygroscopic at the SGP site, and contained up to ~ 18-fold volume increase in water compared to dry particles depending on chemical composition of particles and metrological conditions.

4 Atmospheric implications

Particle liquid water content influences many atmospheric processes. For example, water in particles facilitates the partitioning of water-soluble gas species into the condensed phase (Blando and Turpin, 2000; Surratt et al., 2006; Ervens et al., 2008; Hennigan et al., 2008; Galloway et al., 2009; Asa-Awuku et al., 2010; Carlton and Turpin, 2013; Hodas et al., 2014). In this study, the growth of nanoparticles (here, the accumulation of the dry species) was simulated with the MABNAG model (Yli-Juuti et al., 2013; Hodshire et al., 2016), in which RH was varied in the range of 30–95 % while concentrations of the dry, gaseous species were kept constant (Fig. 9). Three new particle formation and growth events simulated with the MABNAG model featured three

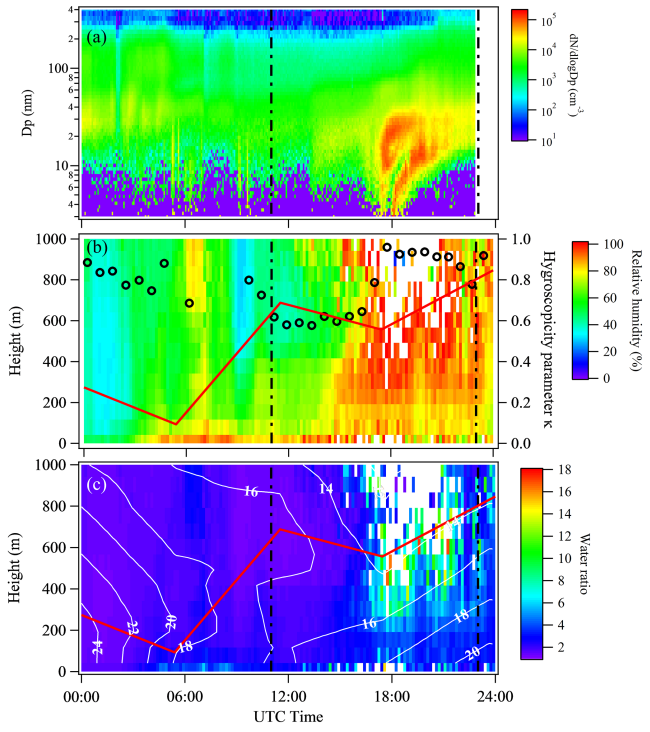

Figure 8. New particle formation event captured by scanning mobility particle sizers **(a)**, vertically and temporally resolved relative humidity **(b)**, and estimated water volume ratio of 13 nm particles **(c)** on 9 May 2013 at SGP. The two vertical dashed lines in each plot represent 06:00 and 18:00 local time, respectively. The red line shows the boundary layer height determined from radiosonde data. Overlaid in the middle plot is the temporally resolved hygroscopicity parameter κ of 13 nm particles obtained by TDMA (open black circles). Temperature (°C) is shown by the white contour lines in the lower plot.

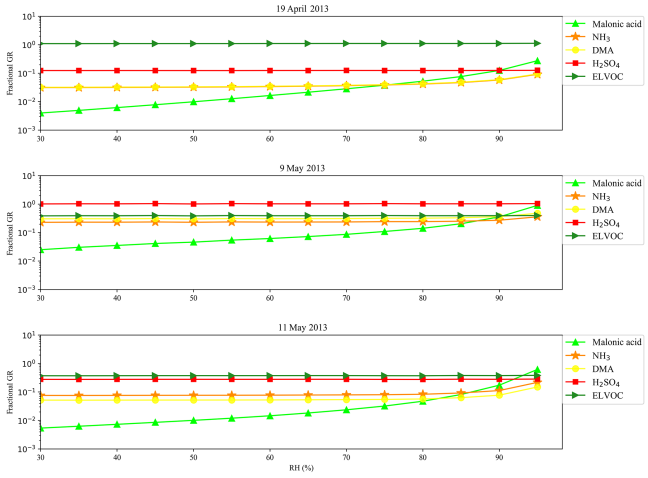

Figure 9. MABNAG prediction of growth rates of 13 nm particles contributed by individual species as a function of relative humidity for three new particle formation events at SGP.

distinct growth pathways. In each case, increased amount of water in nanoparticles at higher RH enhances the partitioning of NH_3, DMA, and organic acids into the condensed phase, but has a negligible effect on the uptake of sulfuric acid and ELVOC, which already have extremely low saturation vapor pressures. Compared to the case of RH 30 %, particle growth by organic acids is enhanced by a factor of 35–100 at RH 95 %, and surpasses growth contributed by sulfuric acid and/or ELVOC in some cases. The modeling results indicate that even for nanometer-sized particles, liquid water content significantly influences the gas-particle partitioning, and therefore chemical composition of particles. Gas species with extremely low saturation vapor pressures dominantly contribute to particle growth at low RH, but water-soluble gas species can be more important to particle growth as RH increases.

Water-soluble gas species (e.g., alcohols, aldehydes, ketones, acids, hydroperoxides, ammonia, amines) also react within particles to form lower volatility species via reactions such as hemiacetal/acetal formation, aldol condensation, salt formation, and esterification (Ervens et al., 2011), though only salt formation is considered in the MABNAG simulations here. The increased partitioning of water-soluble gas species in ultrafine particles may substantially increase the growth of particles and yield of secondary organic aerosol (SOA) through these mechanisms. The partitioning of water-soluble oxidizing species like hydroperoxides in ultrafine particles also increases the oxidizing capacity of particles, and enhances aqueous-phase oxidation processes, impacting SOA formation. In addition, it is well known that H_2O_2 causes significant damage to human lung cells (Gurtner et al., 1987; Oosting et al., 1990; Holm et al., 1991; Sporn et al., 1992). Ultrafine particles associated with increased H_2O_2 can penetrate deeply into the lung and impair lung function to a greater extent. Therefore, considering liquid water content in ultrafine particles in modeling studies is of great importance for accurately estimating particle growth, atmospheric chemical reaction rates, SOA formation, and the effects of particles on human health.

5 Conclusions

In summary, we measured vertical profiles of particle number concentrations in the size range of 11–16 nm with a tethered balloon system at the US Department of Energy ARM SGP field site in Oklahoma. These observations were compared with simultaneous ground-based data obtained from three scanning mobility particle sizers to understand the vertical extent of new particle formation. We found that new particle formation was initiated at the top region of the boundary layer, and subsequently mixed downward to ground level in 0.5–1 h due to the strong vertical mixing on the NPF event day of 12 May 2013. The ground-based TDMA data indicate that newly formed particles at the SGP site are highly hy-

groscopic and typically contain up to 50 % water by volume depending on chemical composition of particles and metrological conditions. During conditions of high RH, liquid water may account for up to 95 % of particle volume for newly formed 13 nm particles. The MABNAG simulation supports the premise that relative humidity, which is vertically and temporally variable, has a substantial effect on the partitioning of gas species into nanoparticles. Specifically, the uptake of organic acids to nanoparticles is greatly enhanced at high RH, and can dominantly contribute to nanoparticle growth. For the current study we focus only on 2 days during which tethered balloon measurements coincided with new particle formation events and 3 days during which we made a comprehensive analysis of nanoparticle growth rates. While we observed a large range of atmospheric conditions as well as nanoparticle properties in our study, additional investigations are needed to assess how representative these days are for general conditions at the SGP site.

While field measurements are commonly performed at ground level, our results highlight the importance of direct measurements of vertically resolved properties of gas species and particles to better understand NPF and growth as well as its impacts on cloud processes and climate. In particular, measurements of the poorly understood water content of nanoparticles would greatly improve modeling studies in gas-particle partitioning and the growth of nanoparticles into submicron-size particles that can serve as CCN.

Data availability. Data were obtained from the Atmospheric Radiation Measurement (ARM) Climate Research Facility, a US Department of Energy Office of Science user facility sponsored by the Office of Biological and Environmental Research. Data from the NPFS field study were last accessed on 20 December 2017 and are freely available from the following data portals: https://www.arm.gov/research/campaigns/sgp2013npfs (NPFS, 2017) and https://www.arm.gov/research/campaigns/sgp2013tbnpfs (TBNPFS, 2017).

Supplement. The supplement related to this article is available online at: https://doi.org/10.5194/acp-18-311-2018-supplement.

Competing interests. The authors declare that they have no conflict of interest.

Acknowledgements. This research was supported by the US Department of Energy's Atmospheric System Research, an Office of Science, Office of Biological and Environmental Research program, under grant no. DE-SC0011780 and grant no. DE-SC0014469. We acknowledge the cooperation of the US Department of Energy's Atmospheric Radiation Measurement (ARM) Climate Research Facility for hosting the NPFS at the Central Facility. We would also like to acknowledge the support of ARM staff at the SGP site, and Professor Don Collins from Texas A & M University for useful discussions regarding the TDMA data. The National Center for Atmospheric Research is operated by the University Corporation for Atmospheric Research under sponsorship from the National Science Foundation. Any opinions, findings, and conclusions or recommendations expressed in this publication are those of the authors and do not necessarily reflect the views of the National Science Foundation.

Edited by: Veli-Matti Kerminen
Reviewed by: two anonymous referees

References

Almeida, J., Schobesberger, S., Kürten, A., Ortega, I. K., Kupiainen-Määttä, O., Praplan, A. P., Adamov, A., Amorim, A., Bianchi, F., Breitenlechner, M., David, A., Dommen, J., Donahue, N. M., Downard, A., Dunne, E., Duplissy, J., Ehrhart, S., Flagan, R. C., Franchin, A., Guida, R., Hakala, J., Hansel, A., Heinritzi, M., Henschel, H., Jokinen, T., Junninen, H., Kajos, M., Kangasluoma, J., Keskinen, H., Kupc, A., Kurtén, T., Kvashin, A. N., Laaksonen, A., Lehtipalo, K., Leiminger, M., Leppä, J., Loukonen, V., Makhmutov, V., Mathot, S., McGrath, M. J., Nieminen, T., Olenius, T., Onnela, A., Petäjä, T., Riccobono, F., Riipinen, I., Rissanen, M., Rondo, L., Ruuskanen, T., Santos, F. D., Sarnela, N., Schallhart, S., Schnitzhofer, R., Seinfeld, J. H., Simon, M., Sipilä, M., Stozhkov, Y., Stratmann, F., Tomé, A., Tröstl, J., Tsagkogeorgas, G., Vaattovaara, P., Viisanen, Y., Virtanen, A., Vrtala, A., Wagner, P. E., Weingartner, E., Wex, H., Williamson, C., Wimmer, D., Ye, P., Yli-Juuti, T., Carslaw, K. S., Kulmala, M., Curtius, J., Baltensperger, U., Worsnop, D. R., Vehkamäki, H., and Kirkby, J.: Molecular understanding of sulphuric acid-amine particle nucleation in the atmosphere, Nature, 502, 359–363, https://doi.org/10.1038/nature12663, 2013.

Andreae, M. O., Afchine, A., Albrecht, R., Holanda, B. A., Artaxo, P., Barbosa, H. M. J., Bormann, S., Cecchini, M. A., Costa, A., Dollner, M., Fütterer, D., Järvinen, E., Jurkat, T., Klimach, T., Konemann, T., Knote, C., Krämer, M., Krisna, T., Machado, L. A. T., Mertes, S., Minikin, A., Pöhlker, C., Pöhlker, M. L., Pöschl, U., Rosenfeld, D., Sauer, D., Schlager, H., Schnaiter, M., Schneider, J., Schulz, C., Spanu, A., Sperling, V. B., Voigt, C., Walser, A., Wang, J., Weinzierl, B., Wendisch, M., and Ziereis, H.: Aerosol characteristics and particle production in the upper troposphere over the Amazon Basin, Atmos. Chem. Phys. Discuss., https://doi.org/10.5194/acp-2017-694, in review, 2017.

Asa-Awuku, A., Nenes, A., Gao, S., Flagan, R. C., and Seinfeld, J. H.: Water-soluble SOA from Alkene ozonolysis: composition and droplet activation kinetics inferences from analysis of CCN activity, Atmos. Chem. Phys., 10, 1585–1597, https://doi.org/10.5194/acp-10-1585-2010, 2010.

Barsanti, K. C., McMurry, P. H., and Smith, J. N.: The potential contribution of organic salts to new particle growth, Atmos. Chem. Phys., 9, 2949–2957, https://doi.org/10.5194/acp-9-2949-2009, 2009.

Barsanti, K. C. and Pankow, J. F.: Thermodynamics of the formation of atmospheric organic particulate matter by accretion reactions – Part 1: Aldehydes and ketones, Atmos. Environ., 38, 4371–4382, https://doi.org/10.1016/j.atmosenv.2004.03.035, 2004.

Benson, D. R., Erupe, M. E., and Lee, S.-H.: Laboratory-measured H_2SO_4-H_2O-NH_3 ternary homogeneous nucleation rates: Initial observations, Geophys. Res. Lett., 36, L15818, https://doi.org/10.1029/2009gl038728, 2009.

Berndt, T., Stratmann, F., Sipilä, M., Vanhanen, J., Petäjä, T., Mikkilä, J., Grüner, A., Spindler, G., Lee Mauldin III, R., Curtius, J., Kulmala, M., and Heintzenberg, J.: Laboratory study on new particle formation from the reaction $OH + SO_2$: influence of experimental conditions, H_2O vapour, NH_3 and the amine tert-butylamine on the overall process, Atmos. Chem. Phys., 10, 7101–7116, https://doi.org/10.5194/acp-10-7101-2010, 2010.

Bilde, M., Barsanti, K., Booth, M., Cappa, C. D., Donahue, N. M., Emanuelsson, E. U., McFiggans, G., Krieger, U. K., Marcolli, C., Topping, D., Ziemann, P., Barley, M., Clegg, S., Dennis-Smither, B., Hallquist, M., Hallquist, Å. M., Khlystov, A., Kulmala, M., Mogensen, D., Percival, C. J., Pope, F., Reid, J. P., Ribeiro da Silva, M. A. V., Rosenoern, T., Salo, K., Soonsin, V. P., Yli-Juuti, T., Prisle, N. L., Pagels, J., Rarey, J., Zardini, A. A., and Riipinen, I.: Saturation vapor pressures and transition enthalpies of low-volatility organic molecules of atmospheric relevance: From dicarboxylic acids to complex mixtures, Chem. Rev., 115, 4115–4156, https://doi.org/10.1021/cr5005502, 2015.

Blando, J. D. and Turpin, B. J.: Secondary organic aerosol formation in cloud and fog droplets: A literature evaluation of plausibility, Atmos. Environ., 34, 1623–1632, https://doi.org/10.1016/S1352-2310(99)00392-1, 2000.

Burkart, J., Willis, M. D., Bozem, H., Thomas, J. L., Law, K., Hoor, P., Aliabadi, A. A., Köllner, F., Schneider, J., Herber, A., Abbatt, J. P. D., and Leaitch, W. R.: Summertime observations of elevated levels of ultrafine particles in the high Arctic marine boundary layer, Atmos. Chem. Phys., 17, 5515–5535, https://doi.org/10.5194/acp-17-5515-2017, 2017.

Carlton, A. G. and Turpin, B. J.: Particle partitioning potential of organic compounds is highest in the Eastern US and driven by anthropogenic water, Atmos. Chem. Phys., 13, 10203–10214, https://doi.org/10.5194/acp-13-10203-2013, 2013.

Chen, H., Varner, M. E., Ezell, M. J., Arquero, K. D., Dawson, M. L., Gerber, R. B., and Finlayson-Pitts, B. J.: New particle formation and growth from methanesulfonic acid, trimethylamine and water, Phys. Chem. Chem. Phys., 17, 13699–13709, https://doi.org/10.1039/C5CP00838G, 2015a.

Chen, H., Varner, M. E., Gerber, R. B., and Finlayson-Pitts, B. J.: Reactions of methanesulfonic acid with amines and ammonia as a source of new particles in air, J. Phys. Chem. B, 1526–1536, https://doi.org/10.1021/acs.jpcb.5b07433, 2015b.

Clegg, S. L., Pitzer, K. S., and Brimblecombe, P.: Thermodynamics of multicomponent, miscible, ionic solutions. II: Mixtures including unsymmetrical electrolytes, J. Phys. Chem., 96, 9470–9479, https://doi.org/10.1021/j100202a074, 1992.

Clegg, S. L. and Seinfeld, J. H.: Thermodynamic models of aqueous solutions containing inorganic electrolytes and dicarboxylic acids at 298.15 K. 1. The acids as nondissociating components, J. Phys. Chem. A, 110, 5692–5717, https://doi.org/10.1021/jp056149k, 2006a.

Clegg, S. L. and Seinfeld, J. H.: Thermodynamic models of aqueous solutions containing inorganic electrolytes and dicarboxylic acids at 298.15 K. 2. Systems including dissociation equilibria, J. Phys. Chem. A, 110, 5718–5734, https://doi.org/10.1021/jp056150j, 2006b.

Collins, D.: Tandem Differential Mobility Analyzer/Aerodynamic Particle Sizer (APS) Handbook, Department of Energy Office of Science Atmospheric Radiation Measurement (ARM) Program (United States), 2010.

Dawson, M. L., Varner, M. E., Perraud, V., Ezell, M. J., Gerber, R. B., and Finlayson-Pitts, B. J.: Simplified mechanism for new particle formation from methanesulfonic acid, amines, and water via experiments and ab initio calculations, P. Natl. Acad. Sci. USA, 109, 18719–18724, https://doi.org/10.1073/pnas.1211878109, 2012.

Donahue, N. M., Trump, E. R., Pierce, J. R., and Riipinen, I.: Theoretical constraints on pure vapor-pressure driven condensation of organics to ultrafine particles, Geophys. Res. Lett., 38, L16801, https://doi.org/10.1029/2011gl048115, 2011.

Donahue, N. M., Ortega, I. K., Chuang, W., Riipinen, I., Riccobono, F., Schobesberger, S., Dommen, J., Baltensperger, U., Kulmala, M., Worsnop, D. R., and Vehkamaki, H.: How do organic vapors contribute to new-particle formation?, Faraday Discuss., 165, 91–104, https://doi.org/10.1039/c3fd00046j, 2013.

Dunne, E. M., Gordon, H., Kürten, A., Almeida, J., Duplissy, J., Williamson, C., Ortega, I. K., Pringle, K. J., Adamov, A., Baltensperger, U., Barmet, P., Benduhn, F., Bianchi, F., Breitenlechner, M., Clarke, A., Curtius, J., Dommen, J., Donahue, N. M., Ehrhart, S., Flagan, R. C., Franchin, A., Guida, R., Hakala, J., Hansel, A., Heinritzi, M., Jokinen, T., Kangasluoma, J., Kirkby, J., Kulmala, M., Kupc, A., Lawler, M. J., Lehtipalo, K., Makhmutov, V., Mann, G., Mathot, S., Merikanto, J., Miettinen, P., Nenes, A., Onnela, A., Rap, A., Reddington, C. L. S., Riccobono, F., Richards, N. A. D., Rissanen, M. P., Rondo, L., Sarnela, N., Schobesberger, S., Sengupta, K., Simon, M., Sipilä, M., Smith, J. N., Stozkhov, Y., Tomé, A., Tröstl, J., Wagner, P. E., Wimmer, D., Winkler, P. M., Worsnop, D. R., and Carslaw, K. S.: Global atmospheric particle formation from CERN CLOUD measurements, Science, 354, 1119–1124, https://doi.org/10.1126/science.aaf2649, 2016.

Ehn, M., Kleist, E., Junninen, H., Petäjä, T., Lönn, G., Schobesberger, S., Dal Maso, M., Trimborn, A., Kulmala, M., Worsnop, D. R., Wahner, A., Wildt, J., and Mentel, Th. F.: Gas phase formation of extremely oxidized pinene reaction products in chamber and ambient air, Atmos. Chem. Phys., 12, 5113–5127, https://doi.org/10.5194/acp-12-5113-2012, 2012.

Ehn, M., Thornton, J. A., Kleist, E., Sipilä, M., Junninen, H., Pullinen, I., Springer, M., Rubach, F., Tillmann, R., Lee, B., Lopez-Hilfiker, F., Andres, S., Acir, I.-H., Rissanen, M., Jokinen, T., Schobesberger, S., Kangasluoma, J., Kontkanen, J., Nieminen, T., Kurten, T., Nielsen, L. B., Jorgensen, S., Kjaergaard, H. G., Canagaratna, M., Maso, M. D., Berndt, T., Petaja, T., Wahner, A., Kerminen, V.-M., Kulmala, M., Worsnop, D. R., Wildt, J., and Mentel, T. F.: A large source of low-volatility secondary organic aerosol, Nature, 506, 476–479, https://doi.org/10.1038/nature13032, 2014.

Ek, M. and Mahrt, L.: Daytime evolution of relative humidity at the boundary layer top, Mon. Weather Rev., 122, 2709–2721, https://doi.org/10.1175/1520-0493(1994)122<2709:DEORHA>2.0.CO;2, 1994.

Erupe, M. E., Viggiano, A. A., and Lee, S.-H.: The effect of trimethylamine on atmospheric nucleation involving H_2SO_4, Atmos. Chem. Phys., 11, 4767–4775, https://doi.org/10.5194/acp-11-4767-2011, 2011.

Ervens, B., Carlton, A. G., Turpin, B. J., Altieri, K. E., Kreidenweis, S. M., and Feingold, G.: Secondary organic aerosol yields from cloud-processing of isoprene oxidation products, Geophys. Res. Lett., 35, L02816, https://doi.org/10.1029/2007gl031828, 2008.

Ervens, B., Turpin, B. J., and Weber, R. J.: Secondary organic aerosol formation in cloud droplets and aqueous particles (aqSOA): a review of laboratory, field and model studies, Atmos. Chem. Phys., 11, 11069–11102, https://doi.org/10.5194/acp-11-11069-2011, 2011.

Facchini, M. C., Mircea, M., Fuzzi, S., and Charlson, R. J.: Cloud albedo enhancement by surface-active organic solutes in growing droplets, Nature, 401, 257–259, https://doi.org/10.1038/45758, 1999.

Farmer, D. K., Cappa, C. D., and Kreidenweis, S. M.: Atmospheric processes and their controlling influence on cloud condensation nuclei activity, Chem. Rev., 115, 4199–4217, https://doi.org/10.1021/cr5006292, 2015.

Finlayson-Pitts, B. J. and Pitts Jr., J. N.: Chemistry of the Upper and Lower Atmosphere: Theory, Experiments, and Applications, Academic Press, San Diego, 2000.

Galloway, M. M., Chhabra, P. S., Chan, A. W. H., Surratt, J. D., Flagan, R. C., Seinfeld, J. H., and Keutsch, F. N.: Glyoxal uptake on ammonium sulphate seed aerosol: reaction products and reversibility of uptake under dark and irradiated conditions, Atmos. Chem. Phys., 9, 3331–3345, https://doi.org/10.5194/acp-9-3331-2009, 2009.

Glasoe, W. A., Volz, K., Panta, B., Freshour, N., Bachman, R., Hanson, D. R., McMurry, P. H., and Jen, C.: Sulfuric acid nucleation: An experimental study of the effect of seven bases, J. Geophys. Res., 120, 1933–1950, https://doi.org/10.1002/2014jd022730, 2015.

Greenberg, J. P., Guenther, A., Zimmerman, P., Baugh, W., Geron, C., Davis, K., Helmig, D., and Klinger, L. F.: Tethered balloon measurements of biogenic VOCs in the atmospheric boundary layer, Atmos. Environ., 33, 855–867, https://doi.org/10.1016/S1352-2310(98)00302-1, 1999.

Greenberg, J. P., Peñuelas, J., Guenther, A., Seco, R., Turnipseed, A., Jiang, X., Filella, I., Estiarte, M., Sardans, J., Ogaya, R., Llusia, J., and Rapparini, F.: A tethered-balloon PTRMS sampling approach for surveying of landscape-scale biogenic VOC fluxes, Atmos. Meas. Tech., 7, 2263–2271, https://doi.org/10.5194/amt-7-2263-2014, 2014.

Gurtner, G. H., Farrukh, I. S., Adkinson Jr., N. F., Sciuto, A. M., Jacobson, J. M., and Michael, J. R.: The role of arachidonate mediators in peroxide-induced lung injury, Am. Rev. Respir. Dis., 136, 480–483, 1987.

Hämeri, K., Väkevä, M., Hansson, H.-C., and Laaksonen, A.: Hygroscopic growth of ultrafine ammonium sulphate aerosol measured using an ultrafine tandem differential mobility analyzer, J. Geophys. Res., 105, 22231–22242, https://doi.org/10.1029/2000jd900220, 2000.

Hämeri, K., Laaksonen, A., Väkevä, M., and Suni, T.: Hygroscopic growth of ultrafine sodium chloride particles, J. Geophys. Res., 106, 20749–20757, https://doi.org/10.1029/2000jd000200, 2001.

Hennigan, C. J., Bergin, M. H., Dibb, J. E., and Weber, R. J.: Enhanced secondary organic aerosol formation due to water uptake by fine particles, Geophys. Res. Lett., 35, L18801, https://doi.org/10.1029/2008gl035046, 2008.

Hodas, N., Sullivan, A. P., Skog, K., Keutsch, F. N., Collett, J. L., Decesari, S., Facchini, M. C., Carlton, A. G., Laaksonen, A., and Turpin, B. J.: Aerosol liquid water driven by anthropogenic nitrate: Implications for lifetimes of water-soluble organic gases and potential for secondary organic aerosol formation, Environ. Sci. Technol., 48, 11127–11136, https://doi.org/10.1021/es5025096, 2014.

Hodshire, A. L., Lawler, M. J., Zhao, J., Ortega, J., Jen, C., Yli-Juuti, T., Brewer, J. F., Kodros, J. K., Barsanti, K. C., Hanson, D. R., McMurry, P. H., Smith, J. N., and Pierce, J. R.: Multiple new-particle growth pathways observed at the US DOE Southern Great Plains field site, Atmos. Chem. Phys., 16, 9321–9348, https://doi.org/10.5194/acp-16-9321-2016, 2016.

Holm, B., Hudak, B., Keicher, L., Cavanaugh, C., Baker, R., Hu, P., and Matalon, S.: Mechanisms of H_2O_2-mediated injury to type II cell surfactant metabolism and protection with PEG-catalase, Am. J. Physiol., 261, C751–C757, 1991.

E-AIM Model: http://www.aim.env.uea.ac.uk/aim/aim.php, last access: 20 December 2017.

Jang, M., Czoschke, N. M., Lee, S., and Kamens, R. M.: Heterogeneous atmospheric aerosol production by acid-catalyzed particle-phase reactions, Science, 298, 814–817, https://doi.org/10.1126/science.1075798, 2002.

Jiang, J., Chen, M., Kuang, C., Attoui, M., and McMurry, P. H.: Electrical mobility spectrometer using a diethylene glycol condensation particle counter for measurement of aerosol size distributions down to 1 nm, Aerosol Sci. Tech., 45, 510–521, https://doi.org/10.1080/02786826.2010.547538, 2011.

Jokinen, T., Sipilä, M., Junninen, H., Ehn, M., Lönn, G., Hakala, J., Petäjä, T., Mauldin III, R. L., Kulmala, M., and Worsnop, D. R.: Atmospheric sulphuric acid and neutral cluster measurements using CI-APi-TOF, Atmos. Chem. Phys., 12, 4117–4125, https://doi.org/10.5194/acp-12-4117-2012, 2012.

Kerminen, V.-M. and Kulmala, M.: Analytical formulae connecting the "real" and the "apparent" nucleation rate and the nuclei number concentration for atmospheric nucleation events, J. Aerosol. Sci., 33, 609–622, https://doi.org/10.1016/S0021-8502(01)00194-X, 2002.

Kerminen, V.-M., Lihavainen, H., Komppula, M., Viisanen, Y., and Kulmala, M.: Direct observational evidence linking atmospheric aerosol formation and cloud droplet activation, Geophys. Res. Lett., 32, L14803, https://doi.org/10.1029/2005gl023130, 2005.

Kirkby, J., Curtius, J., Almeida, J., Dunne, E., Duplissy, J., Ehrhart, S., Franchin, A., Gagné, S., Ickes, L., Kürten, A., Kupc, A., Metzger, A., Riccobono, F., Rondo, L., Schobesberger, S., Tsagkogeorgas, G., Wimmer, D., Amorim, A., Bianchi, F., Breitenlechner, M., David, A., Dommen, J., Downard, A., Ehn, M., Flagan, R. C., Haider, S., Hansel, A., Hauser, D., Jud, W., Junninen, H., Kreissl, F., Kvashin, A., Laaksonen, A., Lehtipalo, K., Lima, J., Lovejoy, E. R., Makhmutov, V., Mathot, S., Mikkilä, J., Minginette, P., Mogo, S., Nieminen, T., Onnela, A., Pereira, P., Petäjä, T., Schnitzhofer, R., Seinfeld, J. H., Sipilä, M., Stozhkov, Y., Stratmann, F., Tomé, A., Vanhanen, J., Viisanen, Y., Vrtala, A., Wagner, P. E., Walther, H., Weingartner, E., Wex, H., Winkler, P. M., Carslaw, K. S., Worsnop, D. R., Baltensperger, U., and Kulmala, M.: Role of sulphuric acid, ammonia and galactic cosmic rays in atmospheric aerosol nucleation, Nature, 476, 429–433, https://doi.org/10.1038/nature10343, 2011.

Korhonen, P., Kulmala, M., Laaksonen, A., Viisanen, Y., McGraw, R., and Seinfeld, J. H.: Ternary nucleation of H_2SO_4, NH_3, and H_2O in the atmosphere, J. Geophys. Res., 104, 26349–26353, https://doi.org/10.1029/1999jd900784, 1999.

Kreidenweis, S. M. and Seinfeld, J. H.: Nucleation of sulfuric acid-water and methanesulfonic acid-water solution particles: Implications for the atmospheric chemistry of organosulfur species, Atmos. Environ., 22, 283–296, https://doi.org/10.1016/0004-6981(88)90034-0, 1988.

Kreidenweis, S. M., Flagan, R. C., Seinfeld, J. H., and Okuyama, K.: Binary nucleation of methanesulfonic acid and water, J. Aerosol. Sci., 20, 585–607, https://doi.org/10.1016/0021-8502(89)90105-5, 1989.

Kreidenweis, S. M., Petters, M. D., and DeMott, P. J.: Single-parameter estimates of aerosol water content, Environ. Res. Lett., 3, 035002, https://doi.org/10.1088/1748-9326/3/3/035002, 2008.

Kuang, C., McMurry, P. H., McCormick, A. V., and Eisele, F. L.: Dependence of nucleation rates on sulfuric acid vapor concentration in diverse atmospheric locations, J. Geophys. Res., 113, D10209, https://doi.org/10.1029/2007jd009253, 2008.

Kuang, C., McMurry, P. H., and McCormick, A. V.: Determination of cloud condensation nuclei production from measured new particle formation events, Geophys. Res. Lett., 36, L09822, https://doi.org/10.1029/2009gl037584, 2009.

Kulmala, M., Vehkamäki, H., Petäjä, T., Dal Maso, M., Lauri, A., Kerminen, V. M., Birmili, W., and McMurry, P. H.: Formation and growth rates of ultrafine atmospheric particles: A review of observations, J. Aerosol. Sci., 35, 143–176, https://doi.org/10.1016/j.jaerosci.2003.10.003, 2004.

Kulmala, M., Kontkanen, J., Junninen, H., Lehtipalo, K., Manninen, H. E., Nieminen, T., Petäjä, T., Sipilä, M., Schobesberger, S., Rantala, P., Franchin, A., Jokinen, T., Järvinen, E., Äijälä, M., Kangasluoma, J., Hakala, J., Aalto, P. P., Paasonen, P., Mikkilä, J., Vanhanen, J., Aalto, J., Hakola, H., Makkonen, U., Ruuskanen, T., Mauldin, R. L., Duplissy, J., Vehkamäki, H., Bäck, J., Kortelainen, A., Riipinen, I., Kurtén, T., Johnston, M. V., Smith, J. N., Ehn, M., Mentel, T. F., Lehtinen, K. E. J., Laaksonen, A., Kerminen, V.-M., and Worsnop, D. R.: Direct observations of atmospheric aerosol nucleation, Science, 339, 943–946, https://doi.org/10.1126/science.1227385, 2013.

Kupiszewski, P., Leck, C., Tjernström, M., Sjogren, S., Sedlar, J., Graus, M., Müller, M., Brooks, B., Swietlicki, E., Norris, S., and Hansel, A.: Vertical profiling of aerosol particles and trace gases over the central Arctic Ocean during summer, Atmos. Chem. Phys., 13, 12405–12431, https://doi.org/10.5194/acp-13-12405-2013, 2013.

Kurtén, T., Loukonen, V., Vehkamäki, H., and Kulmala, M.: Amines are likely to enhance neutral and ion-induced sulfuric acid-water nucleation in the atmosphere more effectively than ammonia, Atmos. Chem. Phys., 8, 4095–4103, https://doi.org/10.5194/acp-8-4095-2008, 2008.

Laakso, L., Grönholm, T., Kulmala, L., Haapanala, S., Hirsikko, A., Lovejoy, E. R., Kazil, J., Kurten, T., Boy, M., and Nilsson, E. D.: Hot-air balloon as a platform for boundary layer profile measurements during particle formation, Boreal Environ. Res., 12, 279–294, 2007.

Lee, S.-H., Reeves, J. M., Wilson, J. C., Hunton, D. E., Viggiano, A. A., Miller, T. M., Ballenthin, J. O., and Lait, L. R.: Particle formation by ion nucleation in the upper troposphere and lower stratosphere, Science, 301, 1886–1889, https://doi.org/10.1126/science.1087236, 2003.

Lewis, E. R.: The effect of surface tension (Kelvin effect) on the equilibrium radius of a hygroscopic aqueous aerosol particle, J. Aerosol. Sci., 37, 1605–1617, https://doi.org/10.1016/j.jaerosci.2006.04.001, 2006.

Limbeck, A., Kulmala, M., and Puxbaum, H.: Secondary organic aerosol formation in the atmosphere via heterogeneous reaction of gaseous isoprene on acidic particles, Geophys. Res. Lett., 30, 1996, https://doi.org/10.1029/2003gl017738, 2003.

McMurry, P. H. and Friedlander, S. K.: New particle formation in the presence of an aerosol, Atmos. Environ., 13, 1635–1651, https://doi.org/10.1016/0004-6981(79)90322-6, 1979.

Merikanto, J., Spracklen, D. V., Mann, G. W., Pickering, S. J., and Carslaw, K. S.: Impact of nucleation on global CCN, Atmos. Chem. Phys., 9, 8601–8616, https://doi.org/10.5194/acp-9-8601-2009, 2009.

Newsom, R.: Doppler Lidar (DL) Handbook, Department of Energy Office of Science Atmospheric Radiation Measurement (ARM) Program (United States), 2012.

NPFS: New Particle Formation Study 2013, data portal: https://www.arm.gov/research/campaigns/sgp2013npfs, last access: 20 December 2017.

Oosting, R. S., van Bree, L., van Iwaarden, J. F., van Golde, L. M., and Verhoef, J.: Impairment of phagocytic functions of alveolar macrophages by hydrogen peroxide, Am. J. Physiol., 259, L87–L94, 1990.

Park, K., Kim, J.-S., and Miller, A. L.: A study on effects of size and structure on hygroscopicity of nanoparticles using a tandem differential mobility analyzer and TEM, J. Nano. Res., 11, 175–183, https://doi.org/10.1007/s11051-008-9462-4, 2009.

Petters, M. D. and Kreidenweis, S. M.: A single parameter representation of hygroscopic growth and cloud condensation nucleus activity, Atmos. Chem. Phys., 7, 1961–1971, https://doi.org/10.5194/acp-7-1961-2007, 2007.

Pierce, J. R. and Adams, P. J.: Efficiency of cloud condensation nuclei formation from ultrafine particles, Atmos. Chem. Phys., 7, 1367–1379, https://doi.org/10.5194/acp-7-1367-2007, 2007.

Pierce, J. R. and Adams, P. J.: Uncertainty in global CCN concentrations from uncertain aerosol nucleation and primary emission rates, Atmos. Chem. Phys., 9, 1339–1356, https://doi.org/10.5194/acp-9-1339-2009, 2009.

Pierce, J. R., Riipinen, I., Kulmala, M., Ehn, M., Petäjä, T., Junninen, H., Worsnop, D. R., and Donahue, N. M.: Quantification of the volatility of secondary organic compounds in ultrafine particles during nucleation events, Atmos. Chem. Phys., 11, 9019–9036, https://doi.org/10.5194/acp-11-9019-2011, 2011.

Pierce, J. R., Leaitch, W. R., Liggio, J., Westervelt, D. M., Wainwright, C. D., Abbatt, J. P. D., Ahlm, L., Al-Basheer, W., Cziczo, D. J., Hayden, K. L., Lee, A. K. Y., Li, S.-M., Russell, L. M., Sjostedt, S. J., Strawbridge, K. B., Travis, M., Vlasenko, A., Wentzell, J. J. B., Wiebe, H. A., Wong, J. P. S., and Macdonald, A. M.: Nucleation and condensational growth to CCN sizes during a sustained pristine biogenic SOA event in a forested mountain valley, Atmos. Chem. Phys., 12, 3147–3163, https://doi.org/10.5194/acp-12-3147-2012, 2012.

Pierce, J. R., Westervelt, D. M., Atwood, S. A., Barnes, E. A., and Leaitch, W. R.: New-particle formation, growth and climate-relevant particle production in Egbert, Canada: analysis from 1

year of size-distribution observations, Atmos. Chem. Phys., 14, 8647–8663, https://doi.org/10.5194/acp-14-8647-2014, 2014.

Riccobono, F., Schobesberger, S., Scott, C. E., Dommen, J., Ortega, I. K., Rondo, L., Almeida, J., Amorim, A., Bianchi, F., Breitenlechner, M., David, A., Downard, A., Dunne, E. M., Duplissy, J., Ehrhart, S., Flagan, R. C., Franchin, A., Hansel, A., Junninen, H., Kajos, M., Keskinen, H., Kupc, A., Kürten, A., Kvashin, A. N., Laaksonen, A., Lehtipalo, K., Makhmutov, V., Mathot, S., Nieminen, T., Onnela, A., Petäjä, T., Praplan, A. P., Santos, F. D., Schallhart, S., Seinfeld, J. H., Sipilä, M., Spracklen, D. V., Stozhkov, Y., Stratmann, F., Tomé, A., Tsagkogeorgas, G., Vaattovaara, P., Viisanen, Y., Vrtala, A., Wagner, P. E., Weingartner, E., Wex, H., Wimmer, D., Carslaw, K. S., Curtius, J., Donahue, N. M., Kirkby, J., Kulmala, M., Worsnop, D. R., and Baltensperger, U.: Oxidation products of biogenic emissions contribute to nucleation of atmospheric particles, Science, 344, 717–721, https://doi.org/10.1126/science.1243527, 2014.

Riipinen, I., Pierce, J. R., Yli-Juuti, T., Nieminen, T., Häkkinen, S., Ehn, M., Junninen, H., Lehtipalo, K., Petäjä, T., Slowik, J., Chang, R., Shantz, N. C., Abbatt, J., Leaitch, W. R., Kerminen, V.-M., Worsnop, D. R., Pandis, S. N., Donahue, N. M., and Kulmala, M.: Organic condensation: a vital link connecting aerosol formation to cloud condensation nuclei (CCN) concentrations, Atmos. Chem. Phys., 11, 3865–3878, https://doi.org/10.5194/acp-11-3865-2011, 2011.

Riipinen, I., Yli-Juuti, T., Pierce, J. R., Petaja, T., Worsnop, D. R., Kulmala, M., and Donahue, N. M.: The contribution of organics to atmospheric nanoparticle growth, Nat. Geosci., 5, 453–458, https://doi.org/10.1038/ngeo1499, 2012.

Rogers, R. R. and Yau, M. K.: A Short Course in Cloud Physics. International Series in Natural Philosophy, 3rd Edn., Elsevier Science, Oxford, UK, 1989.

Seinfeld, J. H. and Pandis, S. N.: Atmospheric Chemistry and Physics: From Air Pollution to Climate Change, John Wiley & Sons, New York, 2006.

Siebert, H., Stratmann, F., and Wehner, B.: First observations of increased ultrafine particle number concentrations near the inversion of a continental planetary boundary layer and its relation to ground-based measurements, Geophys. Res. Lett., 31, L09102, https://doi.org/10.1029/2003gl019086, 2004.

Sipilä, M., Berndt, T., Petäjä, T., Brus, D., Vanhanen, J., Stratmann, F., Patokoski, J., Mauldin, R. L., Hyvärinen, A.-P., Lihavainen, H., and Kulmala, M.: The role of sulfuric acid in atmospheric nucleation, Science, 327, 1243–1246, https://doi.org/10.1126/science.1180315, 2010.

Sivaraman, C., McFarlane, S., Chapman, E., Jensen, M., Toto, T., Liu, S., and Fischer, M.: Planetary Boundary Layer (PBL) Height Value Added Product (VAP): Radiosonde Retrievals, Department of Energy Office of Science Atmospheric Radiation Measurement (ARM) Program (United States), 2013.

Smith, J. N., Barsanti, K. C., Friedli, H. R., Ehn, M., Kulmala, M., Collins, D. R., Scheckman, J. H., Williams, B. J., and McMurry, P. H.: Observations of aminium salts in atmospheric nanoparticles and possible climatic implications, P. Natl. Acad. Sci. USA, 107, 6634–6639, https://doi.org/10.1073/pnas.0912127107, 2010.

Sporn, P., Marshall, T. M., and Peters-Golden, M.: Hydrogen peroxide increases the availability of arachidonic acid for oxidative metabolism by inhibiting acylation into phospholipids in the alveolar macrophage, Am. J. Respir. Cell Mol., 7, 307–316, 1992.

Spracklen, D. V., Carslaw, K. S., Kulmala, M., Kerminen, V.-M., Sihto, S.-L., Riipinen, I., Merikanto, J., Mann, G. W., Chipperfield, M. P., Wiedensohler, A., Birmili, W., and Lihavainen, H.: Contribution of particle formation to global cloud condensation nuclei concentrations, Geophys. Res. Lett., 35, L06808, https://doi.org/10.1029/2007gl033038, 2008.

Stolzenburg, M. R., McMurry, P. H., Sakurai, H., Smith, J. N., Mauldin, R. L., Eisele, F. L., and Clement, C. F.: Growth rates of freshly nucleated atmospheric particles in Atlanta, J. Geophys. Res., 110, D22S05, https://doi.org/10.1029/2005jd005935, 2005.

Stratmann, F., Siebert, H., Spindler, G., Wehner, B., Althausen, D., Heintzenberg, J., Hellmuth, O., Rinke, R., Schmieder, U., Seidel, C., Tuch, T., Uhrner, U., Wiedensohler, A., Wandinger, U., Wendisch, M., Schell, D., and Stohl, A.: New-particle formation events in a continental boundary layer: first results from the SATURN experiment, Atmos. Chem. Phys., 3, 1445–1459, https://doi.org/10.5194/acp-3-1445-2003, 2003.

Surratt, J. D., Kroll, J. H., Kleindienst, T. E., Edney, E. O., Claeys, M., Sorooshian, A., Ng, N. L., Offenberg, J. H., Lewandowski, M., Jaoui, M., Flagan, R. C., and Seinfeld, J. H.: Evidence for organosulfates in secondary organic aerosol, Environ. Sci. Technol., 41, 517–527, https://doi.org/10.1021/es062081q, 2006.

Svenningsson, B., Rissler, J., Swietlicki, E., Mircea, M., Bilde, M., Facchini, M. C., Decesari, S., Fuzzi, S., Zhou, J., Mønster, J., and Rosenørn, T.: Hygroscopic growth and critical supersaturations for mixed aerosol particles of inorganic and organic compounds of atmospheric relevance, Atmos. Chem. Phys., 6, 1937–1952, https://doi.org/10.5194/acp-6-1937-2006, 2006.

TBNPFS: Tethered Balloon Launches During NPFS2013, data portal: https://www.arm.gov/research/campaigns/sgp2013tbnpfs, last access: 20 December 2017.

Turner, D.: Raman lidar (RL) handbook, Department of Energy Office of Science Atmospheric Radiation Measurement (ARM) Program (United States), 2009.

Wang, J., Krejci, R., Giangrande, S., Kuang, C., Barbosa, H. M. J., Brito, J., Carbone, S., Chi, X., Comstock, J., Ditas, F., Lavric, J., Manninen, H. E., Mei, F., Moran-Zuloaga, D., Pöhlker, C., Pöhlker, M. L., Saturno, J., Schmid, B., Souza, R. A. F., Springston, S. R., Tomlinson, J. M., Toto, T., Walter, D., Wimmer, D., Smith, J. N., Kulmala, M., Machado, L. A. T., Artaxo, P., Andreae, M. O., Petäjä, T., and Martin, S. T.: Amazon boundary layer aerosol concentration sustained by vertical transport during rainfall, Nature, 539, 416–419, https://doi.org/10.1038/nature19819, 2016.

Weber, R. J., Marti, J. J., McMurry, P. H., Eisele, F. L., Tanner, D. J., and Jefferson, A.: Measured atmospheric new particle formation rates: Implications for nulceation mechanisms, Chem. Eng. Commun., 151, 53–64, https://doi.org/10.1080/00986449608936541, 1996.

Weber, R. J., Marti, J. J., McMurry, P. H., Eisele, F. L., Tanner, D. J., and Jefferson, A.: Measurements of new particle formation and ultrafine particle growth rates at a clean continental site, J. Geophys. Res., 102, 4375–4385, https://doi.org/10.1029/96jd03656, 1997.

Weber, R. J., McMurry, P. H., Mauldin, R. L., Tanner, D. J., Eisele, F. L., Clarke, A. D., and Kapustin, V. N.: New particle formation in the remote troposphere: A comparison of ob-

servations at various sites, Geophys. Res. Lett., 26, 307–310, https://doi.org/10.1029/1998gl900308, 1999.

Weber, R. J., Chen, G., Davis, D. D., Mauldin III, R. L., Tanner, D. J., Eisele, F. L., Clarke, A. D., Thornton, D. C., and Bandy, A. R.: Measurements of enhanced H_2SO_4 and 3–4 nm particles near a frontal cloud during the First Aerosol Characterization Experiment (ACE 1), J. Geophys. Res., 106, 24107–24117, 2001.

Wehner, B., Siebert, H., Stratmann, F., Tuch, T., Wiedensohler, A., Petäjä, T., Dal Maso, M., and Kulmala, M.: Horizontal homogeneity and vertical extent of new particle formation events, Tellus B, 59, 362–371, https://doi.org/10.1111/j.1600-0889.2007.00260.x, 2007.

Westervelt, D. M., Pierce, J. R., Riipinen, I., Trivitayanurak, W., Hamed, A., Kulmala, M., Laaksonen, A., Decesari, S., and Adams, P. J.: Formation and growth of nucleated particles into cloud condensation nuclei: model–measurement comparison, Atmos. Chem. Phys., 13, 7645–7663, https://doi.org/10.5194/acp-13-7645-2013, 2013.

Wexler, A. S. and Clegg, S. L.: Atmospheric aerosol models for systems including the ions H^+, NH_4^+, Na^+, SO_4^{2-}, NO_3^-, Cl^-, Br^-, and H_2O, J. Geophys. Res., 107, 4207, https://doi.org/10.1029/2001jd000451, 2002.

Woodward, J. L.: Estimating the Flammable Mass of a Vapor Cloud, John Wiley & Sons, Hoboken, NJ, USA, 2010.

Wyslouzil, B. E., Seinfeld, J. H., Flagan, R. C., and Okuyama, K.: Binary nucleation in acid-water systems. II. Sulfuric acid–water and a comparison with methanesulfonic acid–water, J. Chem. Phys., 94, 6842–6850, https://doi.org/10.1063/1.460262, 1991a.

Wyslouzil, B. E., Seinfeld, J. H., Flagan, R. C., and Okuyama, K.: Binary nucleation in acid-water systems. I. Methanesulfonic acid–water, J. Chem. Phys., 94, 6827–6841, https://doi.org/10.1063/1.460261, 1991b.

Yli-Juuti, T., Barsanti, K., Hildebrandt Ruiz, L., Kieloaho, A.-J., Makkonen, U., Petäjä, T., Ruuskanen, T., Kulmala, M., and Riipinen, I.: Model for acid-base chemistry in nanoparticle growth (MABNAG), Atmos. Chem. Phys., 13, 12507–12524, https://doi.org/10.5194/acp-13-12507-2013, 2013.

Yu, H., McGraw, R., and Lee, S.-H.: Effects of amines on formation of sub-3 nm particles and their subsequent growth, Geophys. Res. Lett., 39, L02807, https://doi.org/10.1029/2011gl050099, 2012.

Zhang, R., Suh, I., Zhao, J., Zhang, D., Fortner, E. C., Tie, X., Molina, L. T., and Molina, M. J.: Atmospheric new particle formation enhanced by organic acids, Science, 304, 1487–1490, https://doi.org/10.1126/science.1095139, 2004.

Zhang, R., Khalizov, A., Wang, L., Hu, M., and Xu, W.: Nucleation and growth of nanoparticles in the atmosphere, Chem. Rev., 112, 1957–2011, https://doi.org/10.1021/cr2001756, 2011.

Zhao, J., Ortega, J., Chen, M., McMurry, P. H., and Smith, J. N.: Dependence of particle nucleation and growth on high-molecular-weight gas-phase products during ozonolysis of α-pinene, Atmos. Chem. Phys., 13, 7631–7644, https://doi.org/10.5194/acp-13-7631-2013, 2013.

Zollner, J. H., Glasoe, W. A., Panta, B., Carlson, K. K., McMurry, P. H., and Hanson, D. R.: Sulfuric acid nucleation: power dependencies, variation with relative humidity, and effect of bases, Atmos. Chem. Phys., 12, 4399–4411, https://doi.org/10.5194/acp-12-4399-2012, 2012.